INTERNATIONAL JOURNAL FOR NUMERICAL AND ANALYTICAL METHODS IN GEOMECHANICS, VOL. 12, 99–116 (1988)

BIFURCATIONS IN FINITE ELEMENT MODELS WITH A NON-ASSOCIATED FLOW LAW

R. DE BORST

TNO Institute for Building Materials and Structures, P.O. Box 49, 2600 AA Delft, The Netherlands

SUMMARY

A numerical approach to bifurcation problems in soil mechanics is described. After locating the bifurcation point by a combination of an incremental-iterative loading procedure and an eigenvalue analysis of the tangent stiffness matrix, the solution is continued on the localization path by a suitable combination of the fundamental solution and the eigenvector belonging to the lowest eigenvalue. The procedures are applied in a bifurcation analysis of a cohesionless soil in a biaxial testing device. The results suggest that a diffuse bifurcation mode with a short wavelength is encountered whereupon a shear band gradually develops. The inclination angle of the shear band compares well with analytical formulae and with empirical data

INTRODUCTION

In recent years, much research effort has been spent to come to a better understanding of bifurcation phenomena in soils. Theoretical contributions of Mandel,[1] Rudnicki and Rice,[2] Vardoulakis[3–5] and Vermeer[6] have greatly enhanced the understanding of shear band formation and of bulging and buckling phenomena. Furthermore, careful experiments by Vardoulakis *et al.*[3] and Arthur *et al.*[7] have provided detailed information about the inclination angle of shear bands in biaxial testing devices.

On the other hand, considerable progress has been made in the application of the finite element method to soil structures. Recent research indicates that it is not only possible to correctly predict stresses and strains in soil bodies under working loads, but that collapse loads can also be computed accurately. Here, special elements have alleviated the problem of locking in plane strain and axisymmetric configurations.[8–11]

The purpose of this paper is to assess the capabilities of numerical techniques to predict bifurcation loads accurately. In addition, we will demonstrate that numerical methods have evolved so far that it is possible to trace the post-peak regime after bifurcation and to simulate localization in soil bodies. Here, numerical methods have definite advantages over analytical methods, since numerical analyses permit continuation of the solution beyond the bifurcation point and computation of the entire load–displacement curve, which is generally not possible using analytical techniques. Furthermore, the generality of the finite element method permits analyses of more complicated configurations than the biaxial test considered here, whereas the applicability of analytical methods is usually limited to relatively simple configurations.

The arrangement of this study is as follows. First, the material model which has been employed is briefly summarized in order to define the variables which are used in the subsequent discussion of theoretical work on bifurcation analyses. Emphasis is placed upon the biaxial test under plane strain conditions since this case has been studied most extensively. Next, the employed numerical

0363-9061/88/010099-18$09.00 *Received 19 January 1987*

procedures are treated. The incremental-iterative solution method is elaborated and the procedures are discussed which have been employed to detect a bifurcation point and to continue the solution after bifurcation. Although the ensuing numerical example pertains to shear band formation in a biaxial testing device, the numerical procedures are completely general and can be used for any other boundary-value problem.

It is finally remarked that the present treatment of the subject matter is by no means exhaustive and that subsequent investigations are needed to shed more light on some questions which could not be solved rigorously within the scope of the present study. For example, the material model which has been employed in the example calculation is relatively simple. Also, the restriction to small displacement gradients which has been made in the present paper must be relaxed in a subsequent investigation.

MATERIAL MODEL

The model which has been adopted in the numerical calculations reported in this paper, is formulated in the spirit of a Mohr–Coulomb plasticity model with a non-associated flow rule. Let f be the yield function, σ_1 be the major and σ_3 be the minor principal stress (tension being taken as positive in accordance with the sign convention in continuum mechanics). Then, the Mohr–Coulomb criterion reads:

$$f=\tfrac{1}{2}(\sigma_1-\sigma_3)+\tfrac{1}{2}(\sigma_1+\sigma_3)\sin\phi_m \tag{1}$$

with ϕ_m the mobilized friction angle. It is noted that a term which accounts for cohesive strength is lacking in equation (1), because we will confine our attention to cohesionless soils in the present paper. The subscript m has been introduced to indicate that ϕ_m is not a constant, but depends on the plastic strain history through a hardening parameter κ. In this study, we have employed as definition for the hardening parameter

$$\kappa=\int\sqrt{(\tfrac{2}{3}\dot{\varepsilon}^p_{ij}\dot{\varepsilon}^p_{ij})}\,\mathrm{d}t \tag{2}$$

with $\dot{\varepsilon}^p_{ij}$ the plastic strain rate tensor and the summation convention being implied. Following Vermeer,[12] the functional relation between the mobilized friction angle ϕ_m and the hardening parameter κ has been assumed to be (Figure 1):

$$\begin{cases} \sin\phi_m=2\dfrac{\sqrt{(\kappa\varepsilon_f)}}{\kappa+\varepsilon_f}\sin\phi & \kappa\leq\varepsilon_f \\ \sin\phi_m=\sin\phi & \kappa>\varepsilon_f \end{cases} \tag{3}$$

with ϕ the value of the friction angle in the limit state. ε_f is the value which κ attains when the frictional strength has been mobilized fully ($\phi_m=\phi$).

The above definition for the hardening parameter κ and the adopted functional dependence of the mobilized friction angle ϕ_m on the hardening parameter κ are not generally accepted. It is well possible that other formulations are more accurate and their choice will certainly affect the results of the analyses quantitatively. For instance, the post-peak response will be different when softening on the mobilized friction angle is employed after the peak friction angle has been reached in place of keeping ϕ_m constant when $\kappa>\varepsilon_f$. Furthermore, the relationship (3) between the mobilized friction angle ϕ_m and κ is rather convex, which implies that a relatively large portion of ε_f is needed to mobilize the last degree of the friction angle ϕ_m up to the limit friction angle ϕ. Nevertheless, the

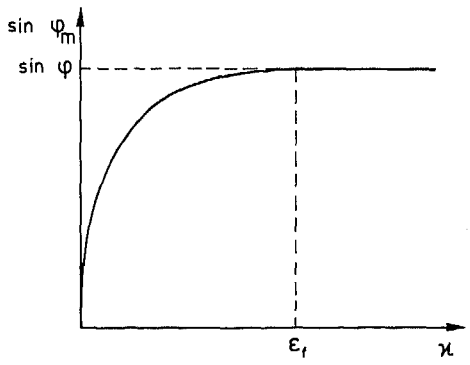

Figure 1. Assumed hardening curve in the employed elastic–plastic model

precise form of relations (2) and (3) seems less important in view of the primary purpose of this paper, i.e. to demonstrate that numerical methods can be used to compute bifurcation points in soil bodies and to trace the load–displacement curve following bifurcation.

The salient departure from classical associated plasticity theory occurs when the plastic strain rates are not obtained by differentiating the yield function f with respect to the stress tensor σ_{ij}, but when $\dot{\varepsilon}^p_{ij}$ is calculated from

$$\dot{\varepsilon}^p_{ij}=\lambda\frac{\partial g}{\partial\sigma_{ij}} \tag{4}$$

with $g\neq f$ and λ a non-negative multiplier. In the computations to be reported in a subsequent section, the definition

$$g=\tfrac{1}{2}(\sigma_1-\sigma_3)+\tfrac{1}{2}(\sigma_1+\sigma_3)\sin\psi_m \tag{5}$$

has been adopted for the plastic potential g. ψ_m is the mobilized dilatancy angle and may also be a function of the plastic strain history (see, for example, Reference 13).

RELATION WITH OTHER STUDIES

The study of stability and bifurcation in elastic–plastic solids was initiated in the late 1950s by a series of fundamental papers by Hill.[14–16] In these studies, attention was primarily devoted to elastic–plastic solids with an associated flow rule and the destabilization was due to geometric effects. A bifurcation analysis for an elastic–plastic solid with a non-associated flow rule (so that bifurcation was triggered by material instability) was first performed by Mandel,[1] who derived that for a Mohr–Coulomb model the critical hardening modulus h_s at which shear band bifurcation is first possible, is given by the expression

$$\frac{h_s}{\mu}=\frac{(\sin\phi_m-\sin\psi_m)^2}{8(1-\nu)} \tag{6}$$

with μ the elastic shear modulus and ν Poisson's ratio. Using different material models, Rudnicki and Rice[2] and Vardoulakis[4] presented analyses similar to that of Mandel.

For a rigid granular material model Vardoulakis[4] furthermore derived an expression for the inclination angle θ of a shear band in a biaxial testing device:

$$\theta=45^\circ+\tfrac{1}{4}(\phi_m+\psi_m) \tag{7}$$

A satisfactory agreement was found between the inclination angle predicted by this formula and experimental data.[3, 7] Later, Vermeer[6] showed that the formula for the inclination angle is rather insensitive with regard to the adopted material model and that the same formula is also obtained for the Mohr–Coulomb friction hardening model considered in this study.

Another important development was the derivation of bifurcation stresses for so-called diffuse bifurcation modes such as bulging and buckling modes,[5, 17, 18] since such bifurcation points may be encountered earlier along the loading path than shear layer bifurcations. In particular, we find that, when specializing Needleman's results[18] for a pressure-sensitive material with a non-dilatant flow rule to a Mohr–Coulomb model and small deformation gradients, such modes first become possible at the elliptic–hyperbolic interface. Then, the hardening modulus h_d is given by

$$\frac{h_d}{\mu}=\tfrac{1}{4}\sin^2\phi_m \tag{8}$$

which coincides with equation (7) for shear band formation when we set $\nu=\frac{1}{2}$ and $\psi_m=0°$. It is interesting to note that at this point diffuse bifurcation modes (symmetric as well as antisymmetric modes) with an arbitrarily short wavelength become available. The importance of these modes for triggering localization in metals has been emphasized by Needleman and Tvergaard.[19] The computational results in this paper suggest that the short wavelength modes may play a similar role in soil bodies.

Strictly speaking, equation (8) is only applicable to materials with incompressible elastic behaviour, since the analyses for the diffuse bifurcation modes pertain either to materials which are elastically and plastically incompressible[17, 18] or to rigid-plastic, dilatant materials.[5] As noted by Needleman and Tvergaard,[19] the elastic compressibility often has a minor influence on the value of the bifurcation stresses and it seems reasonable to suppose that the conclusion that, for elastically incompressible materials, diffuse modes with an arbitrarily short wavelength emerge simultaneously with localized shear band modes at least supports the assertion that, for elastically compressible materials, shear band modes and short wavelength modes will occur virtually simultaneously.

Another approach to bifurcation problems is to simulate the loading process numerically. In metal plasticity this approach was pioneered by Needleman and Tvergaard,[19] while localization analyses on soil samples have been presented by Vermeer and de Borst[12] and Prévost.[20] Yet, these analyses should not be considered as true bifurcation analyses, since the biaxial test was simulated by introducing a small imperfection in the model, either material[20] or geometrical.[12] In doing so, the correct inclination angle of a shear band can perhaps be found, but a proper assessment of the critical hardening modulus at which bifurcation is first possible cannot be made because introduction of a small imperfection transfers the bifurcation problem to a limit problem. Consequently, the limit load which is found depends on the particular imperfection which is introduced.

COMPUTATIONAL PROCEDURES

Uniqueness of solution of a discrete mechanical system can be assessed by considering incremental equilibrium

$$\int_V \mathbf{B}^{\mathrm{T}}\dot{\boldsymbol{\sigma}}\,\mathrm{d}V=\dot{\mu}\mathbf{q}^* \tag{9}$$

In (9), $\mathbf{B}$ is the strain-nodal displacement matrix, $\dot{\boldsymbol{\sigma}}$ is the stress rate vector, $\dot{\mu}$ is the loading rate, and

$\mathbf{q}^*$ is a normalized load vector. The superscript T is used to denote a transpose. Suppose that there would be another stress rate distribution, which would result from the loading rate $\dot{\mu}$ and which would also satisfy incremental equilibrium. The *difference* $\Delta\dot{\boldsymbol{\sigma}}$ of both stress rate distributions would then satisfy the condition

$$\int_V \mathbf{B}^T \Delta\dot{\boldsymbol{\sigma}}\, dV = \mathbf{0} \tag{10}$$

Introducing an incrementally-linear solid

$$\dot{\boldsymbol{\sigma}} = \mathbf{D}\dot{\boldsymbol{\varepsilon}} \tag{11}$$

with $\mathbf{D}$ the matrix which contains the tangential moduli and $\dot{\boldsymbol{\varepsilon}}$ the strain rate vector, and defining the strain rate–nodal velocity relation

$$\dot{\boldsymbol{\varepsilon}} = \mathbf{B}^T \dot{\boldsymbol{\alpha}} \tag{12}$$

we can rewrite equation (10) as

$$\int_V \mathbf{B}^T \mathbf{D}\mathbf{B}\, dV \Delta\dot{\boldsymbol{\alpha}} = \mathbf{0} \tag{13}$$

with $\Delta\dot{\boldsymbol{\alpha}}$ the difference between both velocity fields. When the stiffness matrix

$$\mathbf{K} = \int_V \mathbf{B}^T \mathbf{D}\mathbf{B}\, dV \tag{14}$$

is introduced, equation (14) changes into

$$\mathbf{K}\Delta\dot{\boldsymbol{\alpha}} = \mathbf{0} \tag{15}$$

A non-trivial solution may then exist if and only if

$$\det(\mathbf{K}) = 0 \tag{16}$$

or equivalently, if at least one eigenvalue of $\mathbf{K}$ vanishes. If a non-trivial solution indeed exists, such a point is named a bifurcation point. It is noted that there is another possibility that $\det(\mathbf{K})$ vanishes. If the load reaches a maximum, $\dot{\mu}$ vanishes, and equation (10) reduces to

$$\mathbf{K}\dot{\boldsymbol{\alpha}} = \mathbf{0} \tag{17}$$

so that for a non-zero vector $\dot{\boldsymbol{\alpha}}$ we also find that equation (16) must be fulfilled (limit point).

In passing from equation (10) to equation (13) it has been tacitly assumed that both strain rates are related to stress rates by the same matrix of tangential moduli $\mathbf{D}$. For elastic-plastic solids, where we have different behaviour in loading and unloading, this is not necessary. Strictly speaking, we have to investigate all possible combinations of loading and unloading to determine whether equation (13) holds for some $\Delta\dot{\boldsymbol{\alpha}}$, since for a non-associated flow rule it is not sufficient to investigate only the case that all plastic points remain on the loading branch due to loss of the variational structure of the field equations.[18]

In a numerical process, a point where the tangent stiffness matrix has a zero eigenvalue cannot be isolated exactly. It has therefore been assumed that a bifurcation point was encountered when the lowest eigenvalue of the tangent stiffness matrix became slightly negative. Since load increments of 0·001 N/mm^2 have been used near bifurcation, the bifurcation point is actually between $-1{\cdot}801$ N/mm^2 and $-1{\cdot}802$ N/mm^2 when we quote a value of $-1{\cdot}802$ N/mm^2 for the bifurcation stress.

When a negative eigenvalue has been calculated, the solution can be continued on the localization path by adding a part of the right eigenvector $\mathbf{v}_1$ belonging to the lowest eigenvalue to

the fundamental solution.[21-23] Let $\Delta\mathbf{a}^*$ be the displacement increment of the fundamental solution. A trial displacement increment $\Delta\mathbf{a}$ for the non-trivial solution can be constructed by taking

$$\Delta\mathbf{a}=\Delta\mathbf{a}^*+\beta\mathbf{v}_1 \tag{18}$$

while the magnitude of the scalar β can be determined from the requirement that

$$\Delta\mathbf{a}^{\mathrm{T}}\Delta\mathbf{a}^*=0 \tag{19}$$

Equation (19) states that the search direction for the non-trivial solution is orthogonal to the fundamental solution. In general, the non-trivial solution will not be in the search direction as defined by equation (19), but when we add equilibrium iterations, condition (19) will maximize the possibility that we converge on the bifurcation path and not on the fundamental solution, although this is not necessarily the lowest bifurcation branch when more equilibrium branches emanate from the bifurcation point. When we do not converge to the lowest bifurcation path, this will be revealed by negative eigenvalues of the bifurcated solution. The above described procedure can then be repeated until we ultimately arrive at the lowest bifurcation path. Substituting equation (19) in (18) yields, after some algebraic manipulations,

$$\Delta\mathbf{a}=\Delta\mathbf{a}^*-\frac{(\Delta\mathbf{a}^*)^{\mathrm{T}}\Delta\mathbf{a}^*}{(\Delta\mathbf{a}^*)^{\mathrm{T}}\mathbf{v}_1}\mathbf{v}_1 \tag{20}$$

Equation (20) fails if the eigenmode is orthogonal to the fundamental path, since the denominator then vanishes. This problem may be resolved by normalizing the trial displacement increment,[21,22] or by setting

$$\Delta\mathbf{a}=\sqrt{[(\Delta\mathbf{a}^*)^{\mathrm{T}}\Delta\mathbf{a}^*]}\mathbf{v}_1 \tag{21}$$

in such cases.

As indicated in the preceding, the tangent stiffness matrix becomes not only singular at bifurcation points, but also at limit points. Both types of behaviour may be encountered in a numerical analysis. For instance, in the case of the biaxial text to be discussed in the next section, a limit point was encountered after first passing a bifurcation point. The most elegant procedure for overcoming limit points is indirect displacement control, which method will be summarized hereafter.

In a nonlinear finite element analysis, the load is applied in a number of small increments. Within each load increment, equilibrium iterations are applied and the iterative improvement $\delta\alpha_i$ in iteration number i to the displacement increment $\Delta\alpha_{i-1}$ is given by

$$\delta\alpha_i=\mathbf{K}_{i-1}^{-1}[\mathbf{p}_{i-1}+\Delta\mu_i\mathbf{q}^*] \tag{22}$$

$\mathbf{K}_{i-1}$ is the possibly updated stiffness matrix, $\mathbf{q}^*$ is a normalized load vector, $\Delta\mu_i$ is the value of the load increment which may change from iteration to iteration and $\mathbf{p}_{i-1}$ is defined by

$$\mathbf{p}_{i-1}=\mu_0\mathbf{q}^*-\int_V \mathbf{B}^{\mathrm{T}}\boldsymbol{\sigma}_{i-1}\,\mathrm{d}V \tag{23}$$

In (23), the symbols μ_0 and $\boldsymbol{\sigma}_{i-1}$ have been introduced for respectively the value of the scalar load parameter at the beginning of the current increment and the stress vector at iteration number $i-1$.

The essence of indirect displacement control is that $\delta\alpha_i$ is conceived to be composed of two contributions

$$\delta\alpha_i=\delta\alpha_i^{\mathrm{I}}+\Delta\mu_i\delta\alpha_i^{\mathrm{II}} \tag{24}$$

with

$$\delta\alpha_i^{\mathrm{I}} = \mathbf{K}_{i-1}^{-1}\mathbf{p}_{i-1} \tag{25}$$

and

$$\delta\alpha_i^{\mathrm{II}} = \mathbf{K}_{i-1}^{-1}\mathbf{q}^* \tag{26}$$

After calculating the displacement vectors $\delta\alpha_i^{\mathrm{I}}$ and $\delta\alpha_i^{\mathrm{II}}$, the value for $\Delta\mu_i$ is determined from some constraint equation on the displacement increments and $\Delta\alpha_i$ is subsequently calculated from

$$\Delta\alpha_i = \Delta\alpha_{i-1} + \delta\alpha_i^{\mathrm{I}} + \Delta\mu_i\delta\alpha_i^{\mathrm{II}} \tag{27}$$

Crisfield,[24] for instance, uses the norm of the incremental displacements as the constraint equation

$$\Delta\alpha_i^{\mathrm{T}}\Delta\alpha_i = \Delta l^2 \tag{28}$$

where Δl is the arc-length of the equilibrium path in the n-dimensional displacement space. The drawback of this so-called spherical arc-length method is that it yields a quadratic equation for the load increment. To circumvent this problem, one may linearize equation (28), which gives[25]

$$\Delta\alpha_i^{\mathrm{T}}\Delta\alpha_{i-1} = \Delta l^2 \tag{29}$$

This method, known as the updated normal path method, results in a linear equation for the load increment. Equation (29) may be simplified further by subtracting the constraint equation of the previous iteration. This gives

$$\Delta\alpha_{i-1}^{\mathrm{T}}(\Delta\alpha_i - \Delta\alpha_{i-2}) = 0 \tag{30}$$

When we furthermore make the approximation

$$\delta\alpha_i \approx 2(\Delta\alpha_i - \Delta\alpha_{i-2}) \tag{31}$$

we obtain

$$\Delta\alpha_{i-1}^{\mathrm{T}}\delta\alpha_i = 0 \tag{32}$$

Substitution of (24) then gives for $\Delta\mu_i$:

$$\Delta\mu_i = -\frac{\Delta\alpha_{i-1}^{\mathrm{T}}\delta\alpha_i^{\mathrm{I}}}{\delta\alpha_{i-1}^{\mathrm{T}}\delta\alpha_i^{\mathrm{II}}} \tag{33}$$

Both equations (28) and (29) have been employed successfully within the realm of geometrically nonlinear problems, where snapping and buckling of thin shells can be traced elegantly. For physically nonlinear problems the method sometimes fails, since failure and bifurcation modes are then often highly localized. Only a few nodes contribute to the norm of displacement increments, and failure is not sensed accurately by a global norm. The constraint equations (28) and (29) are therefore amended by applying weights to the different degrees-of-freedom or omitting some of them from the constraint equation. Equation (29) then changes into

$$\Delta\mathbf{u}_i^{\mathrm{T}}\Delta\mathbf{u}_{i-1} = \Delta l^2 \tag{34}$$

where $\Delta\mathbf{u}_i$ contains only a limited number of the degrees-of-freedom of those of $\Delta\alpha_i$, and equation (33) changes in a similar fashion. In the example of a biaxial test to be discussed in a subsequent section, the load has been applied to the top of the sample, while the magnitude of the load was determined by constraining the displacement increment of the top of the sample.[21,22] Dependence relations in which some degrees-of-freedom are forced to follow the displacement of a 'master' degree-of-freedom, have been employed to ensure that all nodal point at the top displaced the same amount, while perfect lubrication has been assumed between the platens and the sample, so that the sample could deform homogeneously.

A final point of attention in this section is the stress point algorithm. Basically, a single-step Euler backward algorithm has been employed to integrate the differential stress–strain law over a loading step, as treated in detail by de Borst and Vermeer.[9] It is noted, however, that for a bifurcation analysis of a biaxial test, the precise nature of the employed stress point algorithm is less important, since prior to the bifurcation point we have a radial stress path. Then, the differences between the various stress point algorithms are usually of minor importance.

COMPUTATIONAL RESULTS

In the numerical analyses, a cohesionless sand has been considered with a Young's modulus $E=100$ N/mm^2, Poisson's ratio $\nu=0{\cdot}2$, $\phi=40°$, $\varepsilon_f=0{\cdot}02$, $\psi_m=0°$ and the confining pressure has been taken equal to $-0{\cdot}4$ N/mm^2. Load incrementation was started from a strain free initial stress state of $\sigma_{xx}=\sigma_{yy}=\sigma_{zz}=-0{\cdot}4$ N/mm^2. After loading the sample to $\sigma_{yy}=-1{\cdot}802$ N/mm^2, which corresponds to a mobilized friction angle $\phi_m=39{\cdot}55°$, a negative eigenvalue was calculated after assembling the tangent stiffness matrix. The corresponding eigenmode has been plotted in Figure 2. We observe a number of waves, quite similar to the wavepattern which is sometimes observed in metal plasticity.[19] The same wavepattern was obtained when the finite element mesh was uniformly refined (Figure 3). Apparently, the bifurcation mode which is associated with this bifurcation point corresponds to a diffuse mode with an arbitrarily short wavelength. We also encounter a first influence of the fineness of the element grid, since comparison of Figures 2 and 3 shows that the number of waves is entirely determined by the number of elements.

The slight non-symmetry in the eigenmodes of Figures 2 and 3 is thought to be caused by the fact that the leftmost node of the lower boundary has been restrained horizontally in order to prevent horizontal translation. The round-off errors and the numerical difficulties in calculating an accurate eigenvector for a non-symmetric system with many degrees-of-freedom may then cause an inaccuracy of the eigenvector. Alternatively, the eigenvectors of Figures 2 and 3 may be linear

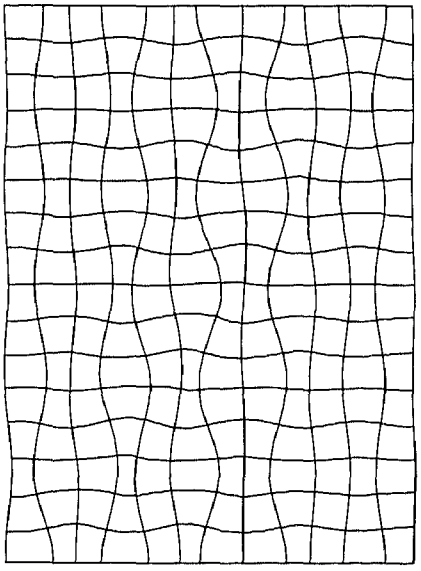

Figure 2. Eigen-displacement field at bifurcation for coarse mesh composed of eight-noded quadrilaterals

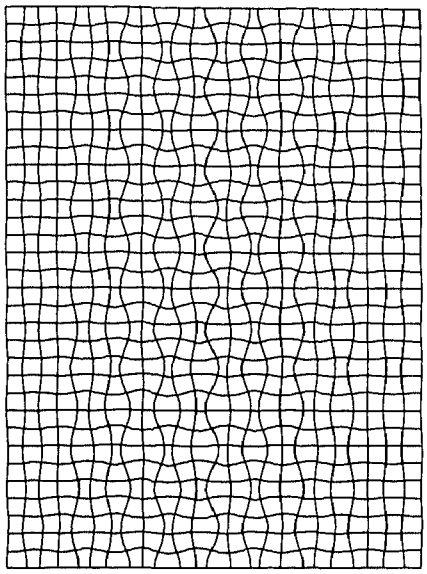

Figure 3. Eigen-displacement field at bifurcation for fine mesh composed of eight-noded quadrilaterals

combinations of symmetric and antisymmetric modes. Needleman[18] has pointed out that symmetric and antisymmetric modes with an arbitrarily short wavelength are both available within the hyperbolic regime. Since, for small deformation gradients, such modes first become available at the elliptic–hyperbolic boundary, symmetric and antisymmetric eigenmodes are both available at this point. Combinations of symmetric and antisymmetric modes are then also eigenvectors, and an eigenvalue analysis of the stiffness matrix at such a point results in an eigenvector which is an arbitrary linear combination of symmetric and antisymmetric modes. Here, it must be mentioned that the eigenvalues have been extracted using a power method. This procedure can only extract the lowest eigenvalue and gives only one eigenvector. More eigenvectors may be obtained when more sophisticated procedures than the power method are employed for extracting the eigenvector.[26] Analyses with advanced eigenvalue algorithms are necessary in order to provide conclusive answers on the questions which have been discussed.

After locating the bifurcation point, the analysis continues as described in the preceding sections, namely by adding a part of the eigenmode to the fundamental solution. The ensuing load–displacement diagram is given in Figure 4, in which we have also plotted the solution which has been obtained for continued homogeneous deformations, i.e. when the solution is obtained without perturbation.

Let us consider the post-bifurcation behaviour of the localized solution in somewhat greater detail (Figure 5). We obtain a stable solution for the localization path after bifurcation, since no negative eigenvalues were calculated for the tangent stiffness matrices in this regime. Subsequent states of stable equilibrium were computed until the load was incremented to $\sigma_{yy} = -1{\cdot}8128$ N/mm^2. After this point, a negative eigenvalue was extracted after assembling the tangent stiffness matrix. A converged solution could not be obtained by incrementing the axial load any further, and use of indirect displacement control resulted in a converged solution at a lower load level. Apparently, the equilibrium path of the localized solution has a limit point for

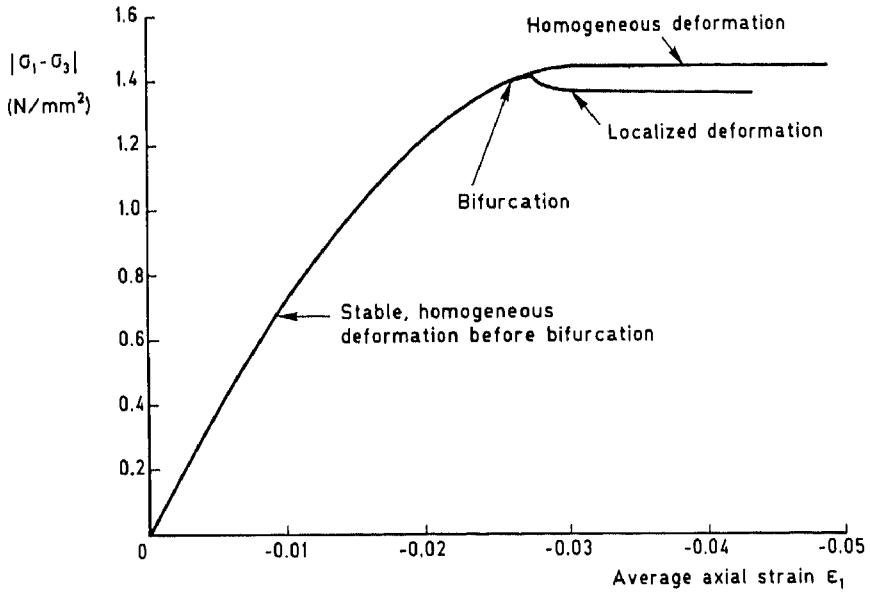

Figure 4. Load–displacement curves of finite element simulations of a biaxial test on a cohesionless material

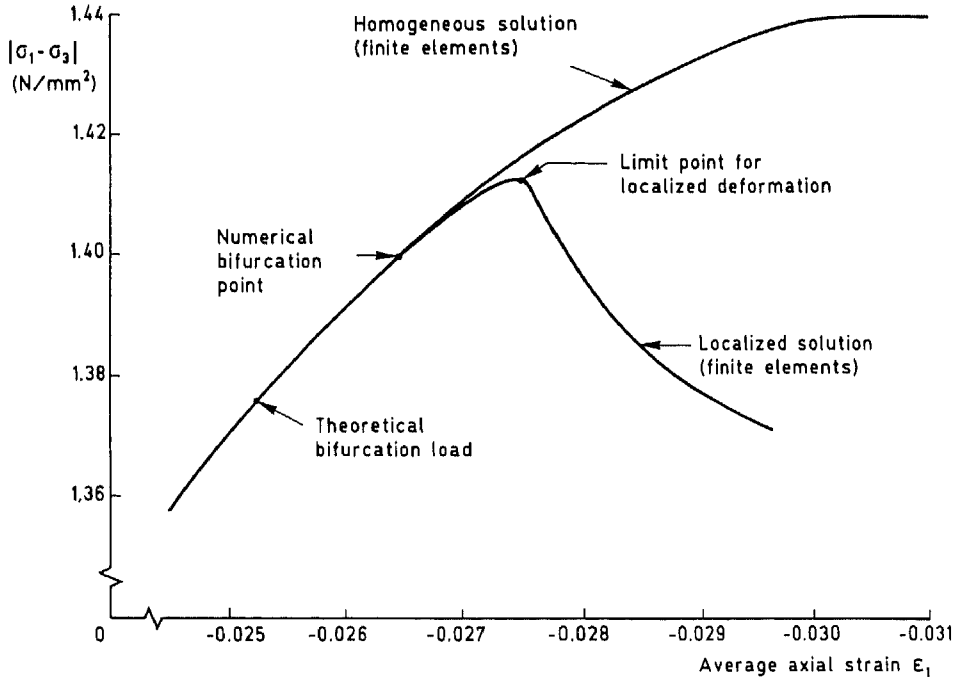

Figure 5. Enlarged graph of finite element results of post-bifurcation behaviour

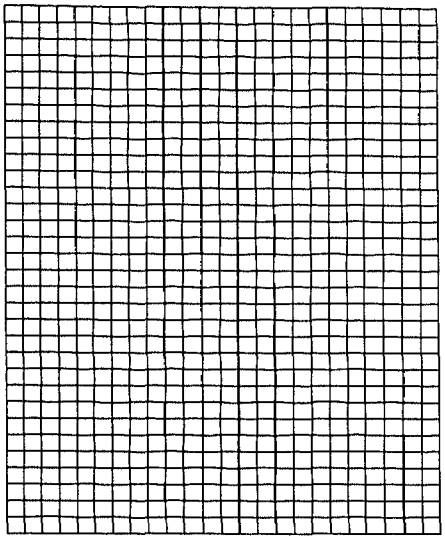

Figure 6. Incremental displacement field immediately after passing the bifurcation point

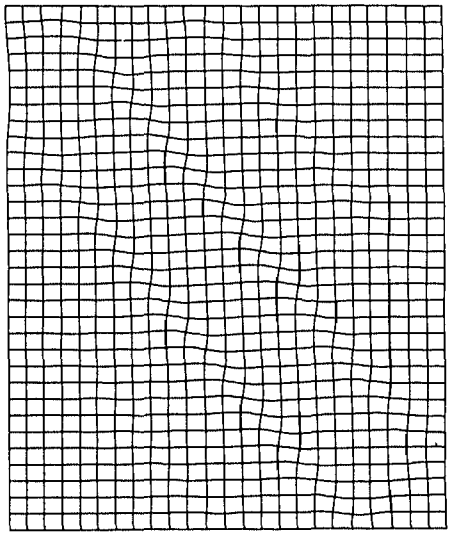

Figure 7. Incremental displacement field after 14 of 26 loading steps on the branch of the non-trivial solution

$\sigma_{yy} = -1{\cdot}8128$ N/mm^2. Continuation of the solution resulted in the descending branch of Figure 5 and ultimately yielded a residual load of $\sigma_{yy} = -1{\cdot}7594$ N/mm^2.

Immediately after bifurcation, the incremental displacement or velocity field is still very similar to the incremental displacement field of the fundamental solution (Figure 6, which results from the calculation with the finer mesh). It is between the bifurcation point and the limit point of the localization path that the shear band gradually develops. First, we observe the development of three zones of localized deformation (Figure 7), but at the limit point of the bifurcation branch all

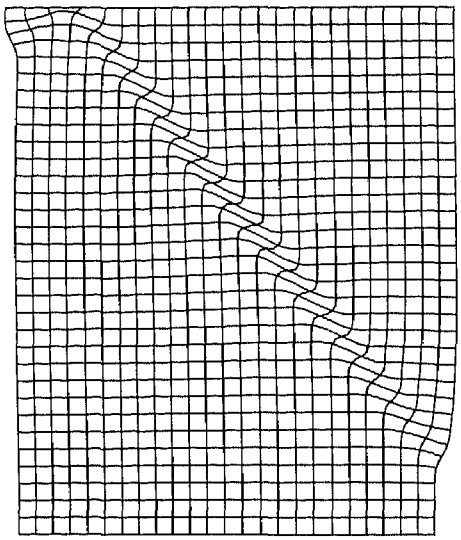

Figure 8. Incremental displacement field at the limit point of the branch of the non-trivial solution (fine mesh composed of eight-noded quadrilaterals)

subsequent deformation is concentrated in one shear layer (Figure 8). The inclination angle of shear band approximately equals 53° which is in reasonable agreement with equation (7) which would predict $\theta \approx 55°$.

The incremental displacement field at the limit point is perhaps the most striking example of the influence of the mesh refinement. Comparing the failure mode of Figure 8 with the failure mode for the coarser mesh (Figure 9), we observe that in both cases the width of the shear zone is completely

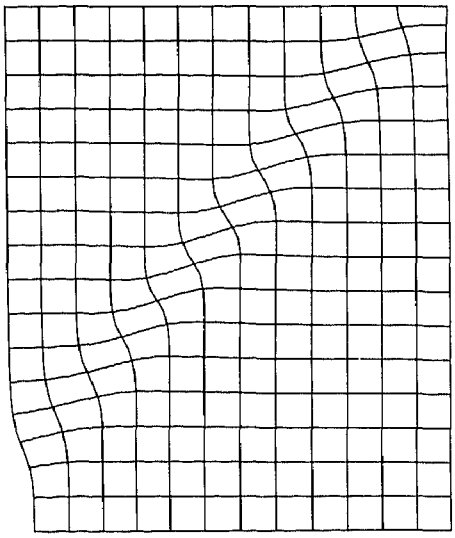

Figure 9. Incremental displacement field at the limit point of the branch of the non-trivial solution (coarse mesh composed of eight-noded quadrilaterals)

determined by the design of the finite element mesh, and is between one element and two elements wide. Equivalent results have been found when studying shear band formation in metals,[19] while similar phenomena have also been observed in crack propagation in concrete. A possible solution to this problem might be the introduction of nonlocal constitutive models.[27,28]

The spacing of the three shear bands which emerge prior to the localization in a single shear layer is probably also governed by the fineness of the finite element discretization. Put differently, the fineness of the element mesh probably determines the number of shear layers which develops initially. Other factors which influence the development of the failure mode are the question of which node at the bottom of the sample is horizontally restrained, the accuracy with which the eigenvector is calculated, and the employed convergence criterion in the first step after bifurcation. The first two factors cause the non-symmetry of the eigenvector and, as a result, the non-symmetry of the incremental displacement field of the non-trivial solution (Figures 6–8). The last factor chiefly determines how many shear layers are found and at which places in the sample they develop. In this context, it is important to note that a completely converged solution could generally not be obtained in the first loading step after forcing bifurcation. After two or three loading steps, full equilibrium could be restored (with, for example, an energy norm $\varepsilon = 10^{-6}$), but in the first step this condition had to be relaxed ($\varepsilon \approx 10^{-3}$).

Of equal importance is the stiffness matrix with which the calculations are carried out. It was found to be necessary to employ a full Newton–Raphson solution procedure, in which the stiffness matrix was reformed and decomposed at each iteration. Iterating with a modified Newton–Raphson procedure caused divergence in this extremely sensitive part of the equilibrium curve, while iterations with the elastic stiffness matrix did not result in convergence to the non-trivial solution, but yielded convergence to the fundamental solution.

CONSEQUENCES OF SPATIAL DISCRETIZATION

The results in the preceding sections have been obtained for the finite element meshes of Figures 10 and 11, which are composed of eight-noded quadrilateral elements. For the coarse mesh of Figure 10 and using 'full' nine-point Gaussian integration, a bifurcation point was computed at a mobilized friction angle $\phi_m = 39{\cdot}55°$. This result is significantly higher than the critical friction angle $\phi_c = 39{\cdot}23°$ which can be computed on basis of equations (3), (7) and (8). In fact, the too 'stiff' behaviour of the numerical analysis is not so surprising in the light of the observations of Nagtegaal *et al.*,[10] who demonstrated that the kinematical constraints which are imposed by the incompressibility constraint for a fully plastic solution, a situation which occurs at complete collapse, may cause 'locking' of elements, thus postponing or even avoiding failure. Eight-noded elements with nine-point integration represent a critical case for planar deformations, in the sense that failure loads can be computed with such an assembly, but that the limit load is usually overestimated unless very fine element divisions are employed. Because of the overstiff behaviour of the displacement based version of the finite element method, the bifurcation load is also overestimated. To alleviate this problem, the use of so-called 'reduced' four-point integration has been advocated,[29] which technique has been widely employed in soil mechanics. Use of such an integration rule resulted in a friction angle $\phi_m = 39{\cdot}41°$ ($\sigma_{yy} = -1{\cdot}791$ N/mm^2), which is appreciably lower than the critical friction angle which was obtained in the analysis with full integration.

Nevertheless, it has been shown that, especially in nonlinear analysis, use of reduced integration may be dangerous.[8,9,21] A nine-point integration rule largely avoids difficulties but, as argued, such a rule results in a too stiff behaviour for plasticity calculations. At present, one of the most reliable techniques seems to be the use of the 15-noded displacement based triangular element with

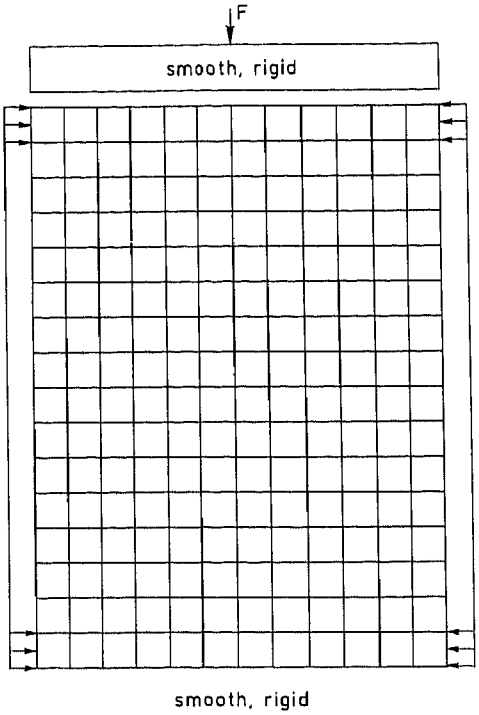

Figure 10. Coarse mesh composed of eight-noded quadrilateral elements

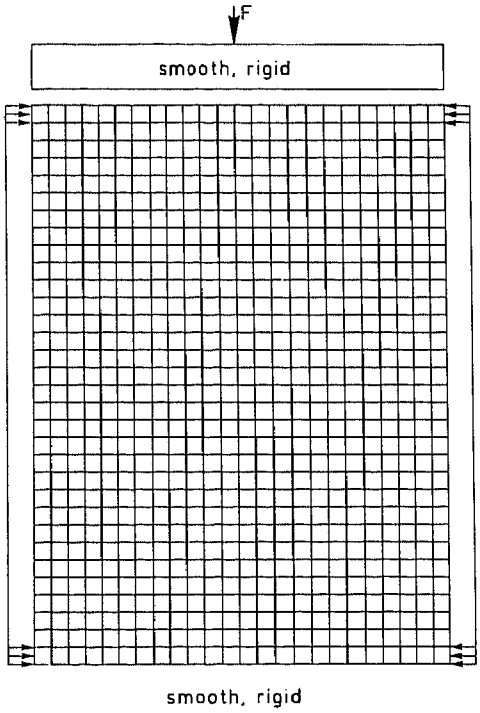

Figure 11. Fine mesh composed of eight-noded quadrilateral elements

a 12-point integration rule.[8,9,11] Repeating the analysis with such an assembly (Figure 13, which has approximately the same number of nodes as the mesh of Figure 10) resulted in a mobilized friction angle $\phi_m = 39{\cdot}31°$ ($\sigma_{yy} = -1{\cdot}783$ N/mm^2), while an analysis with a coarser mesh (Figure 12) resulted in $\phi_m = 39{\cdot}48°$ ($\sigma_{yy} = 1{\cdot}797$ N/mm^2), which is still lower than the results with nine-point integration for the much finer mesh of Figure 10. The fact that for the triangles a lower bifurcation load was obtained for the finer mesh confirms the well-known fact that the numerical solution converges to the 'true' solution upon mesh refinement. The results for the bifurcation load for the different assemblies are summarized in Figure 14.

A final remark concerns the relatively small differences between the various friction angles; for example, the difference between the friction angle at which shear band bifurcation is theoretically possible and the limit friction angle amounts to less than 2 per cent. This is caused by the convex relationship (3) between $\sin \phi_m$ and the hardening parameter κ. Indeed, when the rate of hardening equals the critical hardening modulus h_c, the mobilized friction angle is less than 2 per cent below the limit friction angle, but the hardening parameter κ is only about 75 per cent of ε_f, i.e. the value which κ attains when $\phi_m = \phi$.

CONCLUSIONS

A method to assess bifurcation loads and post-bifurcation behaviour of soil structures with aid of finite elements has been described. It consists of a combination of an incremental-iterative procedure to reach the bifurcation point and an eigenvalue analysis of the tangent stiffness matrix to determine the bifurcation point. Since a non-associated plasticity model has been used, the

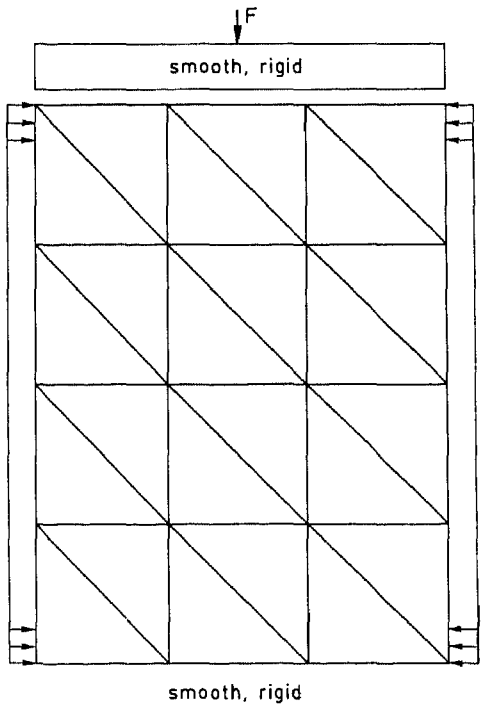

Figure 12. Coarse mesh composed of 15-noded triangular elements

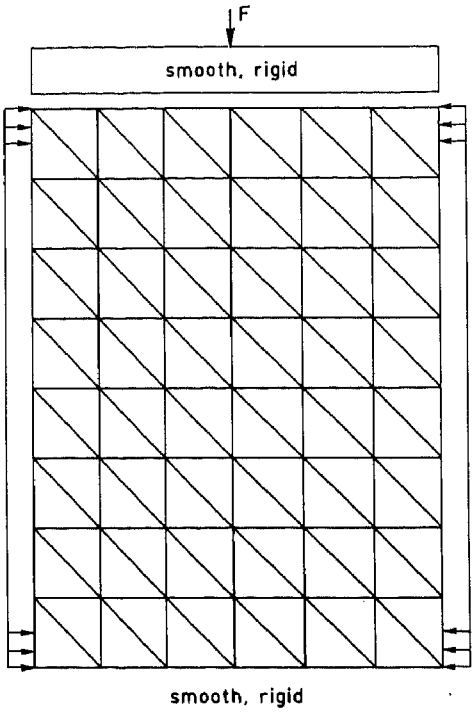

Figure 13. Fine mesh composed of 15-noded triangular elements

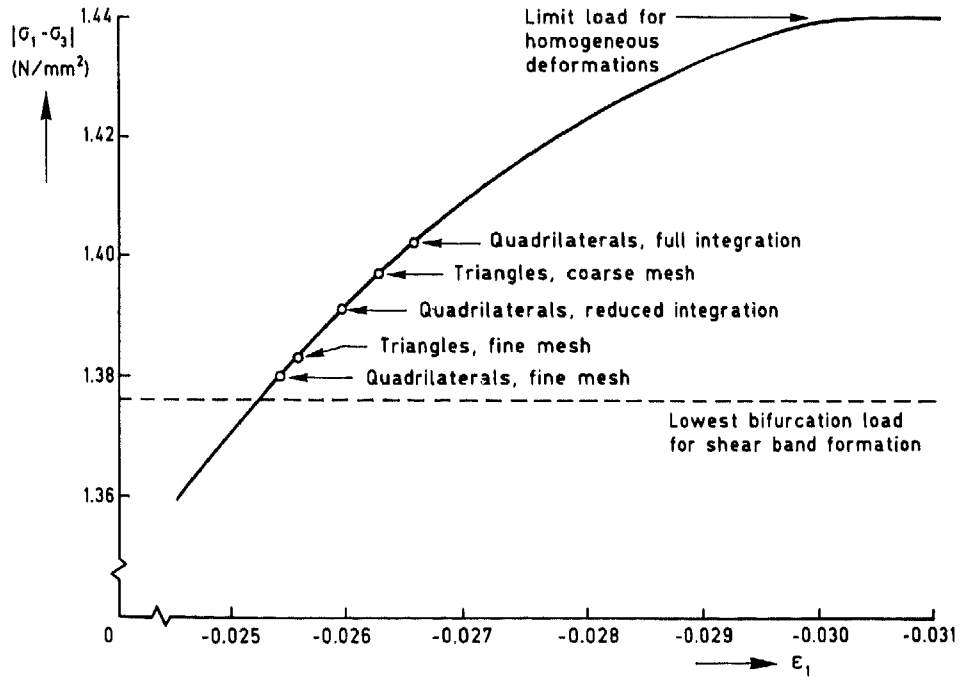

Figure 14. Bifurcation points for different discretizations

tangent stiffness matrix became non-symmetric. When the lowest eigenvalue of the tangent stiffness matrix became (slightly) negative, the solution was continued on the bifurcation path by a suitable combination of the fundamental solution and the right eigenvector which corresponds to the lowest eigenvalue. Before as well as beyond the bifurcation point, the solution has been controlled by indirect displacement control.[21, 22, 24, 25]

The numerical procedures have been applied to a biaxial test on dry sand. The results suggest that a diffuse bifurcation mode with an arbitrarily short wavelength is encountered first along the equilibrium path. After forcing bifurcation, three shear layers initially developed for the finest discretization, which at the limit point of the branch of the non-trivial solution culminated in one shear band. The inclination angle of this shear band corresponds well with the analytical solution.[6]

A serious problem which emerges in the present study as well as in related studies on other materials,[19, 30, 31] is the strong mesh-dependence. While for the material model used in this study the possible impact on the limit load was not noticeable, the calculated deformation patterns and the evolution of the failure pattern were clearly governed by the fineness of the element discretization.

The present study once more underlines the importance of using elements which do not suffer from 'locking' in incompressible solids. In the context of soil mechanics, where we not only have the possibility of plastic incompressibility, but also of plastic dilatancy, the 15-noded displacement based triangle[8, 9, 11] appears to be quite competitive.

It is finally noted that the observed post-bifurcation behaviour will probably significantly depend on the adopted mechanical model. Another material model or inclusion of large displacement effects may well change the precise outcome of the analysis.

ACKNOWLEDGEMENTS

The author wishes to express his gratitude to Dr. Pieter A. Vermeer of Delft University of Technology, Department of Civil Engineering for the fruitful discussions he shared with him on this topic. The calculations reported in this paper have been performed with the DIANA finite element code on the VAX 11/780 computer of the TNO Institute for Building Materials and Structures.

REFERENCES

1. J. Mandel, 'Conditions the stabilité et postulat de Drucker', in *Proc. IUTAM Symp. on Rheology and Soil Mechanics* (Eds. J. Kravtchenko and P. M. Sirieys), Springer-Verlag, Berlin, 1966, pp. 58–68.
2. J. W. Rudnicki and J. R. Rice, 'Conditions of the localization of the deformation in pressure-sensitive materials', *J. Mech. Phys. Solids*, **23**, 371–394 (1975).
3. I. Vardoulakis, M. Goldscheider and G. Gudehus, 'Formation of shear bands in sand bodies as a bifurcation problem', *Int. j. numer. anal. methods geomech.*, **2**, 99–128 (1978).
4. I. Vardoulakis, 'Shear band inclination and shear modulus of sand in biaxial tests', *Int. j. numer. anal. methods geomech.*, **4**, 103–119 (1980).
5. I. Vardoulakis, 'Bifurcation analysis of the plane rectilinear deformations in dry sand', *Int. J. Solids Struct.*, **17**, 1085–1011 (1981).
6. P. A. Vermeer, 'A simple shear-band analysis using compliances', in *Proc. IUTAM Symp. Deformation and Failure of Granular Materials* (Eds. P. A. Vermeer and H. J. Luger), Balkema Publ., Rotterdam, 1982, pp. 493–499.
7. J. R. F. Arthur, T. Dunstan, Q. A. J. Al-Ani and A. Assadi, 'Plastic deformation and failure in granular media', *Géotechnique*, **27**, 53–74 (1977).
8. R. de Borst, 'Calculation of collapse loads using higher order elements', in *Proc. IUTAM Symp. Deformation and Failure of Granular Materials* (Eds. P. A. Vermeer and H. J. Luger), Balkema Publ., Rotterdam, 1982, pp. 503–513.
9. R. de Borst and P. A. Vermeer, 'Possibilities and limitations of finite elements for limit analysis', *Géotechnique*, **34**, 199–210 (1984).

10. J. C. Nagtegaal, D. M. Parks and J. R. Rice, 'On numerically accurate finite element solutions in the fully plastic range', *Comp. Meth. Appl. Mech. Eng.*, **4**, 113–135 (1974).
11. S. W. Sloan and M. F. Randolph, 'Numerical prediction of collapse loads using finite element methods', *Int. j. numer. anal. methods geomech.*, **6**, 47–76 (1982).
12. P. A. Vermeer and R. de Borst, 'Non-associated plasticity for soils, concrete and rock, *Heron*, **29** (3), 1–62 (1984).
13. P. A. Vermeer, 'A double hardening model for sand', *Géotechnique*, **28**, 413–433 (1978).
14. R. Hill, 'A general theory of uniqueness and stability in elastic–plastic solids', *J. Mech. Phys. Solids*, **6**, 236–249 (1958).
15. R. Hill, 'Some basic principles in the mechanics of solids without a natural time', *J. Mech. Phys. Solids*, **7**, 209–225 (1959).
16. R. Hill, 'Acceleration waves in solids', *J. Mech. Phys. Solids*, **10**, 1–16 (1962).
17. R. Hill and J. W. Hutchinson, 'Bifurcation phenomena in the plane tension test', *J. Mech. Phys. Solids*, **23**, 239–264 (1975).
18. A. Needleman, 'Non-normality and bifurcation in plane strain tension and compression', *J. Mech. Phys. Solids*, **27**, 231–254 (1979).
19. A. Needleman and V. Tvergaard, 'Finite element analysis of localization in plasticity', in *Finite Elements: Special Problems in Solid Mechanics* (Eds. J. T. Oden and G. F. Carey), Ch. 5, Prentice-Hall, New Jersey, 1984, pp. 94–157.
20. J. H. Prévost, 'Localization of deformation in elastic–plastic solids', *Int. j. numer. anal. methods geomech.*, **8**, 187–196 (1984).
21. R. de Borst, 'Non-linear analysis of frictional materials', *Dissert.*, Delft Univ. of Technology, Delft (1986).
22. R. de Borst, 'Computation of post-bifurcation and post-failure behavior of strain-softening solids', *Comp. Struct.*, **25**, 211–224 (1987).
23. E. Riks, 'An incremental approach to the solution of snapping and buckling problems', *Int. J. Solids Struct.*, **15**, 529–551 (1979).
24. M. A. Crisfield, 'A fast incremental/iterative procedure that handles snap-through'. *Comp. Struct.*, **13**, 55–62 (1981).
25. E. Ramm, 'The Riks/Wempner approach—an extension of the displacement control method in nonlinear analyses', in *Recent Advances in Non-Linear Computational Mechanics* (Eds. E. Hinton, D. R. J. Owen and C. Taylor), Ch. 3, Pineridge Press, Swansea, UK, 1982, pp. 63–86.
26. G. H. Golub and C. F. Van Loan, *Matrix Computations*, The John Hopkins Univ. Press, Baltimore, 1983.
27. Z. P. Bažant, T. B. Belytschko and T.-P. Chang, 'Continuum theory for strain softening', *J. Eng. Mech., A.S.C.E.*, **110**, 1666–1692 (1984).
28. H. L. Schreyer and Z. Chen, 'One-dimensional softening with localization', *J. Appl. Mech.*, **53**, 791–797 (1986).
29. O. C. Zienkiewicz, C. Humpheson and R. W. Lewis, 'Associated and non-associated visco-plasticity and plasticity in soil mechanics', *Géotechnique*, **25**, 671–689 (1975).
30. Z. P. Bažant and L. Cedolin, 'Blunt crack band propagation in finite element analysis', *J. Eng. Mech. Div., A.S.C.E.*, **105**, 297–315 (1979).
31. J. G. Rots, P. Nauta, G. M. A. Kusters and J. Blaauwendraad, 'Smeared crack approach and fracture localization in concrete', *Heron*, 30(1), 1–48 (1984).